iScience

CellPress
OPEN ACCESS

Article

Electrical energy storage using compressed gas in depleted hydraulically fractured wells

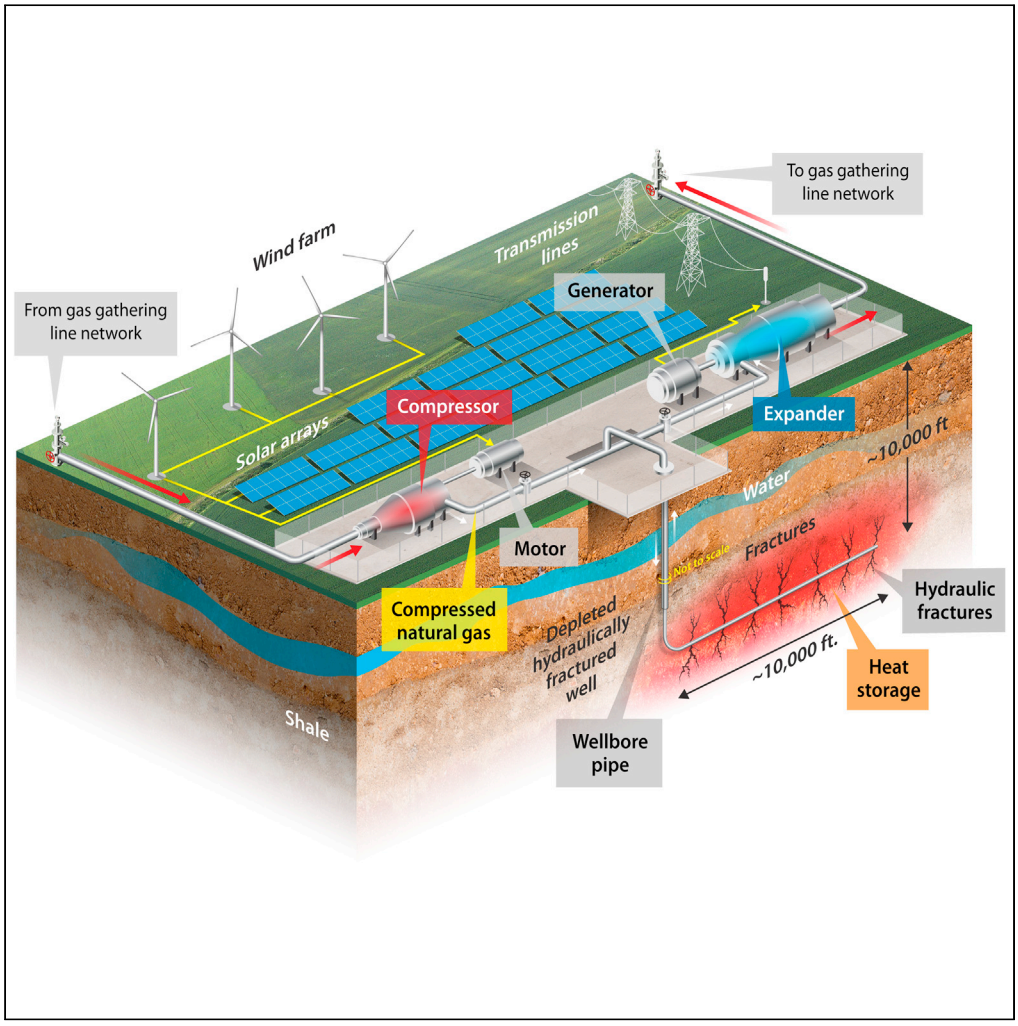

David L. Young, Henry Johnston, Chad Augustine

david.young@nrel.gov

Highlights

REpurposed hydraulically FRActured wells for Energy Storage (REFRAES) is modeled

REFRAES compresses natural gas (or N_2, CO_2, or H_2) instead of air into the well

Thermal energy from gas compression is stored in the well for increased efficiency

Seasonal round-trip efficiency can be as high as 70% at grid-level scale (TWh)

Young et al., iScience 24, 103459
December 17, 2021
https://doi.org/10.1016/j.isci.2021.103459

iScience

CellPress
OPEN ACCESS

Article

Electrical energy storage using compressed gas in depleted hydraulically fractured wells

David L. Young,[1,2,*] Henry Johnston,[1] and Chad Augustine[1]

SUMMARY

Renewable forms of electricity generation like solar and wind require low-cost energy storage solutions to meet climate change deployment goals. Here, we explore the use of depleted hydraulically fractured ("fracked") oil and gas wells to store electrical energy in the form of compressed natural gas to be released to spin an expander/generator when electrical demand is high. Our reservoir model indicates that the same dual-porosity geological environment of fracked wells used to liberate hydrocarbons is also suitable for storing and releasing gas in a diurnal or seasonal cycle. Round-trip storage efficiency is calculated to be 40%–70% depending on the natural reservoir temperature. Levelized cost of storage is estimated to be $70–270/MWh, on par with pumped hydro storage. This study indicates that repurposed "fracked" wells could provide a much-needed low-cost seasonal energy storage solution at the TWh scale.

INTRODUCTION

As electrical grids diversify to renewable energy technologies to decrease costs or avoid carbon production, low-cost storage solutions will be needed to time-shift the energy both daily and seasonally to coincide with peak demands (Alternative Renewables Cost Assumptions in Annual Energy Outlook 2020, 2020; Fu et al., 2018; Haegel et al., 2019). The United States had 2.2 GW of installed energy storage capacity in 2019 which increased 10× to 23.2 GW in 2020, and this is projected to grow to over 70 GW by 2030 and nearly 180 GW by 2040 (Blakers et al., 2019),(BNEF, 2019; Center for Sustainable Systems, 2020). Compressed air energy storage (CAES) projects store electricity by using off-demand power to run compressors to inject air into man-made salt caverns in salt domes, but could also use hard rock or porous rock caverns or existing mines or saline aquifers(Succar and Williams, 2008). The pressurized air is stored until electricity demand is high; then, the air is forced through a turboexpander to generate electricity. Due to the Joule–Thomson effect, the expanding air cools significantly and would form water droplets or ice crystals if not for a small amount of natural gas added to the air stream and combusted prior to expansion. The two existing CAES plants in the US and Germany use 40% less natural gas per kilowatt (kW) of power produced compared to a gas turbine due to the energy stored and returned by CAES and have been operating cost effectively for more than 20 years (Succar and Williams, 2008). Additionally, CAES plants reduce CO_2 emissions by 40%–60% compared to traditional gas-fired plants and operate at 42%–55% efficiency (Energy Storage Association, 2020). Unfortunately, CAES plants are geographically limited owing to the need for geological salt dome formations or off-shore saline aquifers (Mouli-Castillo et al., 2019).

This paper explores a new idea for electrical energy storage that is similar to CAES but uses depleted or nearly depleted *hydraulically fractured wells* instead of salt dome formations to store compressed *natural gas* that can be released to spin an expander/generator when electrical demand is high (Augustine et al., 2021b). We call this new technology REFRAES (REpurposed FRAcked wells for Energy Storage).

The idea, as shown in Figure 1, differs from conventional CAES in salt caverns in three ways:

1. It uses compressed natural gas as the energy storage medium instead of air,
2. It uses unconventional shale and tight sandstone dry gas wells that have been hydraulically fractured (fracked) and depleted to store energy as compressed natural gas,

[1]National Renewable Energy Laboratory, Golden, CO 80401, USA

[2]Lead contact

*Correspondence: david.young@nrel.gov

https://doi.org/10.1016/j.isci.2021.103459

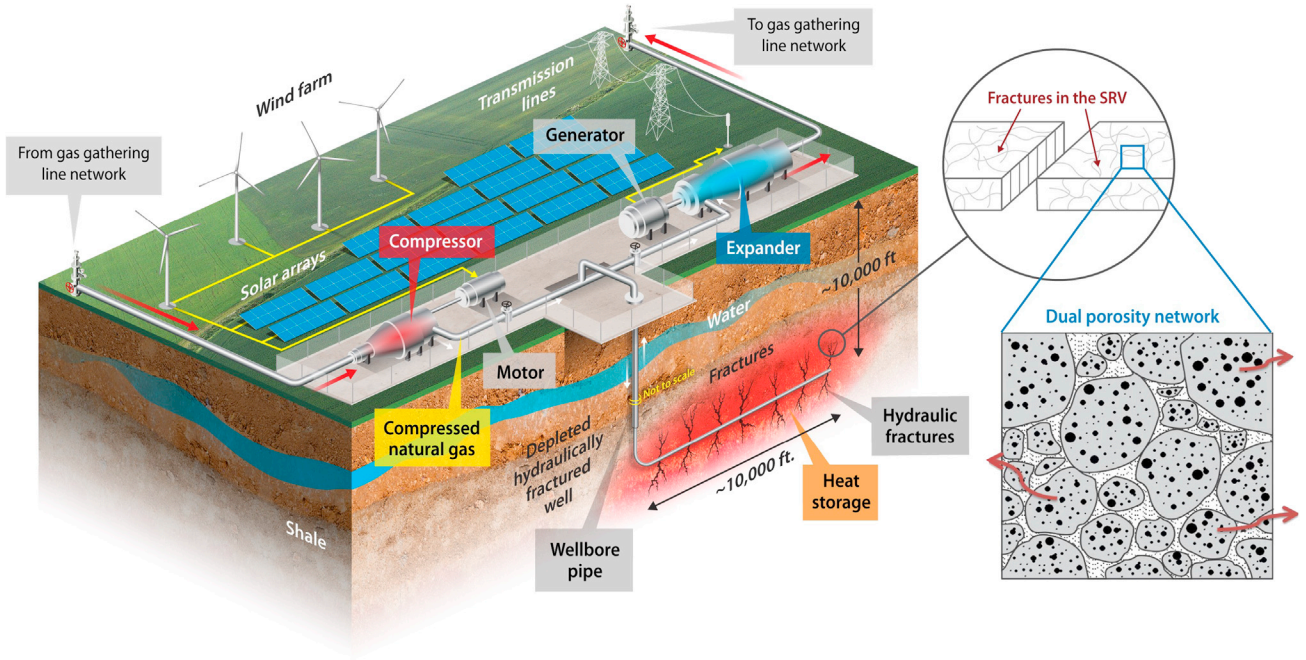

Figure 1. Schematic illustrating the REFRAES process

3. It stores thermal energy from the compression stage by injecting the hot gas directly into the well and storing it in the subsurface formation. This increases the energy content of the stored gas and overall cycle efficiency.

REFRAES uses the existing infrastructure of hydraulically fractured well sites, takes pressurized natural gas from gathering (sales) line pipes in an oil and gas field, and compresses the gas back down the well hole using electrical energy from excess renewable sources. When electrical energy is called for, the gas is released from the well and sent through a turboexpander/generator *unburned* to produce electricity and then sent back to the gathering line manifold where it can be processed. The gas does not have to be combusted during the expansion process because unlike salt domes that must remain relatively cool for structural stability; the heat of compression can be captured in the subsurface formation and the natural geothermal temperature gradient of the well and stored. Released gas from the reservoir is hot enough to not cool below the dew point during expansion, thus avoiding droplet formation while increasing round-trip efficiency.

In addition to the efficient, carbon-free storage cycle, the proposed concept has several other advantages over conventional CAES including a larger number of available sites spread geographically across the U.S., lower risks in reservoir development, and lower capital costs. Few locations possess suitable geology for conventional CAES development, and mining subsurface storage reservoirs (e.g., salt dome caverns) carries inherent project risk and uncertainty that can derail projects (Schulte et al., 2012). Hydraulically fractured wells are spread throughout the United States and, serendipitously, are co-located with abundant wind and solar resources in the West but smaller renewable resources in the East (see Figure 2 and Ref (DOE, 2021; Roberts, 2021 and USGS, 2021) for more detailed maps). The number of active horizontal, hydraulically fractured wells in the United States has grown from about 9,000 in 2000 to more than 250,000 in 2017(US Energy Information Administration, 2019) and continues to grow. There is significant unconventional shale development with a high density of wells in California (power company: CalISO), Colorado (Xcel), Texas (ERCOT), and the Eastern Midwest (PJM).

The trend in drilling horizontal wells has been to drill multiple wells from a single pad. One of the reasons for so many wells is that each well tends to significantly decline in production over a short period of time (Hughes, 2014; Lake et al., 2013; Wachtmeister et al., 2017). For example, wells in the Eagle Ford, Marcellus,

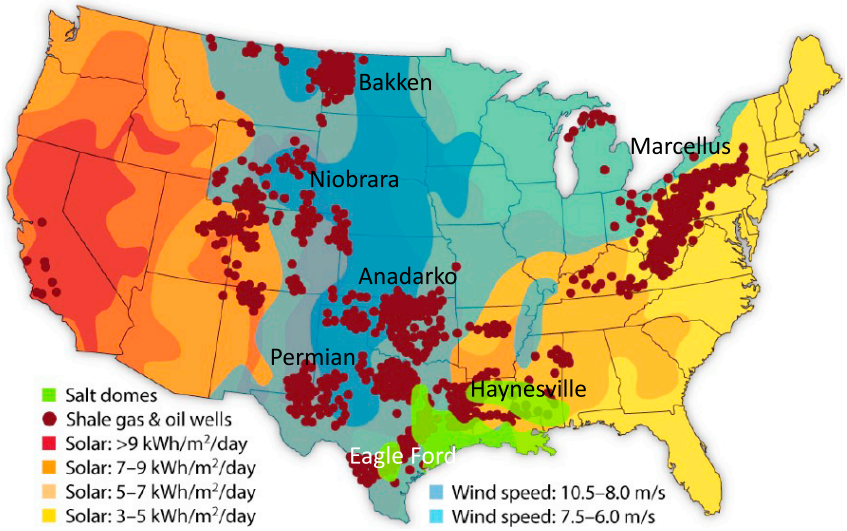

Figure 2. Co-location of wind resources, solar resources, and unconventional shale wells that could be used for REFRAES

and Bakken shale plays decline in oil production by ~70% in the first year (US Energy Information Administration, 2011; Lund, 2014; Wachtmeister et al., 2017). Synergistically, so many wells nearing the end of their profitable lifetime could provide the necessary energy storage capacity within the REFRAES concepts. Additionally, these wells are already drilled, fractured, and completed with a known production history so they can be easily vetted for energy storage suitability prior to the start of any construction, greatly reducing geologic risk to the project. In contrast, the only two conventional CAES plants in the world are the Huntorf CAES plant, a 290 MW facility located near Bremen, Germany completed in 1978; and the McIntosh plant, a 110 MW facility in southwestern Alabama, U.S. completed in 1991(Succar and Williams, 2008). These >100 MW projects required investments of hundreds of millions of dollars to build out their unique surface hardware and geologic infrastructure. REFRAES, on the other hand, leverages existing surface and geological infrastructure, reducing projects costs to only a few million dollars per well. In addition, hardware can be shared over multiple wells and the energy storage capacity expanded by ganging together neighboring wells sharing common drill pads (typically 4–12, but as many as 24–64 wells per pad) (Gupta and Turaga, 2021) and across gas fields to other pads. The use of natural gas, available from existing wells and gathering pipelines on site, avoids potential corrosion and combustion concerns from using air (oxygen) down a hydrocarbon producing well. Indeed, some hydraulically fractured wells are currently being pressurized with gathering line natural gas to enhance oil recovery (EOR) (Atan et al., 2018). Transitioning wells to a REFRAES configuration by adding a compressor and an expander to the surface hardware provides economic incentive to well-owners by generating revenue from electrical energy generation at peak demand periods. Although the goal of renewable energy storage is to reduce or eliminate fossil fuels, we recognize that many integrated assessment (Van Vuuren et al., 2018) and energy mix (Birol, 2021) models include fossil fuels in energy mix scenarios for as far out as 2050 and thus the natural gas infrastructure will likely remain during the global transition from fossil fuels to renewable energy. The use of gathering line natural gas should be considered a gateway gas to transition wells to REFRAES, as other gases could also be used within the closed cycle system (e.g. CO_2, H_2, or N_2) (Raziperchikolaee and Mishra, 2019). All told, the REFRAES idea allows oil/gas energy companies to turn underproducing wells from stranded liabilities to money-producing assets, with a very low carbon energy storage cycle. It may also offer incentive for companies to claim abandoned ("orphaned") wells that are typically a liability for area governments (Kim, 2021; Turrentine, 2021).

In this study, we developed models for the three main steps in the REFRAES process: 1) compression/expansion in the surface plant, 2) injection/production through the wellbore, and 3) storage in the shale reservoir— and integrated them to evaluate the performance of the REFRAES process (Figure 3). The sections below describe each of the models. The ability to predict and control injection and production of natural gas into and from a shale reservoir through a hydraulically fractured well is one of the most important

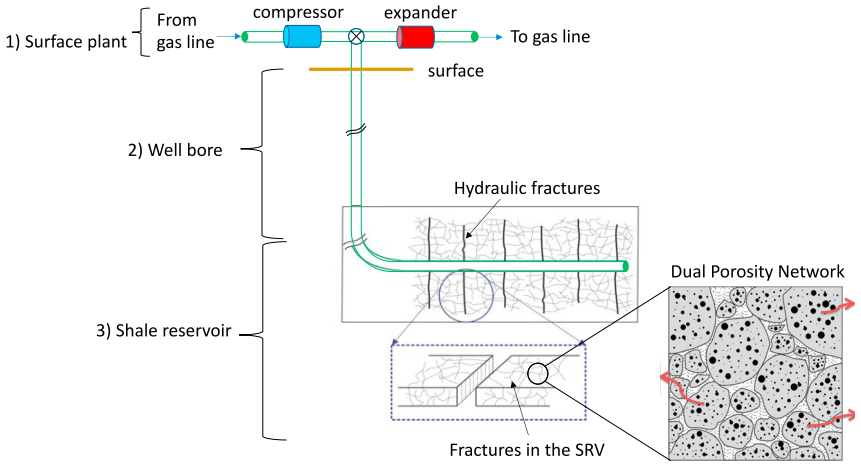

Figure 3. Schematic diagram of the three modeled parts of the REFRAES energy storage system: 1) the surface plant, 2) the vertical wellbore, and 3) the hydraulically fractured reservoir network

and challenging aspects of the REFRAES concept. In an earlier study, using data from dry gas shale plays such as the Marcellus, Haynesville, and Barnett, we completed extensive reservoir modeling(Augustine et al., 2021a) for the injection and production flow rates, pressures, temperatures, and reservoir response during cyclic injection and production of natural gas under energy storage operations. The gas injection occurs near the natural reservoir temperature, pressure, and flow rate, so reservoir deterioration is unlikely. Likewise, the natural gas/water mixture produced from the well will not be significantly altered from normal well production other than potentially gradually drying out with each storage cycle. Using the reservoir model results here we developed a model for gas flow in the wellbore that accounts for pressure and thermal energy losses. We also modeled compression/expansion in the surface plant equipment to estimate power consumption and generation. We then combined the results of the reservoir model to wellbore and surface plant modeling to analyze an integrated system of the REFRAES process. Through parametric analysis, we determined the key factors affecting energy storage performance for two scenarios: a short-term (diurnal) cycle with six hours of storage and a long-term (seasonal) cycle with 90 days of energy storage. This latter seasonal cycle is of great importance for addressing long-term energy storage needs in the U.S (Albertus et al., 2020). As highlighted in section 6 and Figure 20 of this paper, REFRAES is one of only a few storage technologies that can store and discharge large quantities of energy over seasonal discharge times. As more intermittent renewable energy sources are connected to the grid, larger and longer-term storage solutions will be needed to avoid curtailment and meet seasonal energy needs. Finally, we estimate the levelized cost of storage for REFRAES based on the modeled performance and estimates of the installed cost of REFRAES equipment. The model predicts that REFRAES is viable and competitive with other utility-scale energy storage technologies.

RESULTS

Reservoir modeling

Hydraulically fractured wells are typically drilled into shale deposits buried several kilometers below the surface. Modern drilling techniques allow wells to extend down to the shale resource and run horizontally through the layer for more than 5 km (Figure 1). Hydraulic fractures are induced at intervals down the length of the horizontal wellbore pipe to crack the shale and create a large network of channels in the rock leading back to the main pipe. Multistage hydraulic fractures create stimulated reservoir volume (SRV) in the wellbore drainage area (Rezaee, 2015). The SRV consists of a network of micro/macro fractures (enhanced through hydraulic stimulation) within the rock matrix, and these fractures have a much higher permeability than the rock matrix (Figure 3). The SRV facilitates the flow of hydrocarbons from small pores of the matrix to fractures in the SRV, to hydraulic fractures, and to the wellbore. When the well begins to flow, fluid in the fractures is produced more quickly than fluids from the matrix; so, production is initially dominated by fracture flow, followed by flow from the matrix through the fractures. Fluid flow and pressure response within the SRV is simulated using a dual-porosity model (Kazemi et al., 2015; Uzun et al., 2016, 2017; Warren and Root, 1963), which accounts for the interactions of flow between the matrix and fracture network with time.

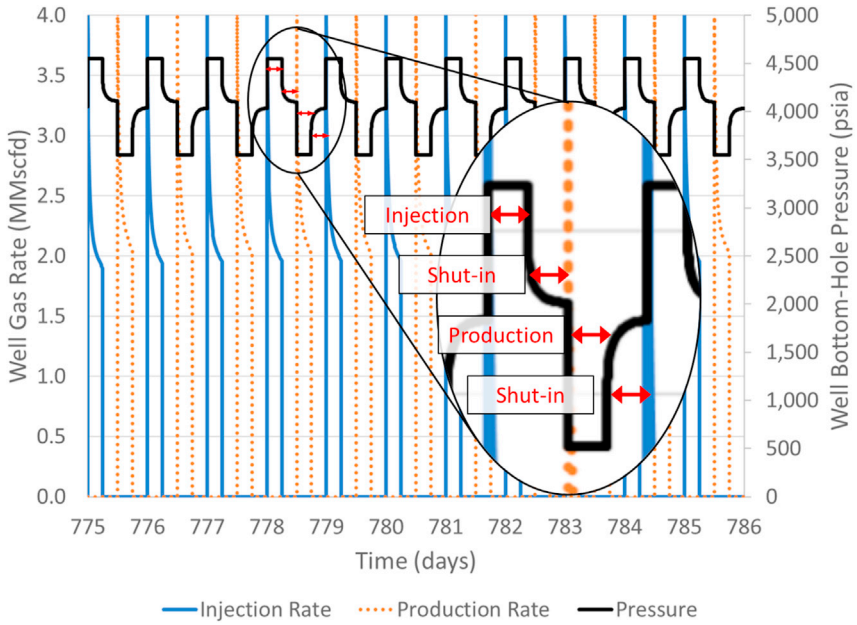

Figure 4. Natural gas injection rate, production rate, and bottomhole pressure during diurnal energy storage cycling. These cycles use an injection bottomhole pressure of 4,500 psi and a production bottomhole pressure of 3,500 psi. The average reservoir pressure at the start of cycling was about 4,000 psi

Modeling this porous network is critical to understanding how shale wells will respond under a REFRAES storage scenario. EOR efforts have demonstrated that natural gas can be injected into and recovered from shale wells. Preliminary calculations show that for the REFRAES idea to be viable, the shale wells must be able to sustain gas flow rates of several million standard cubic feet per day (MMscfd) (typical for most wells) while simultaneously keeping the difference between the injection and production wellhead pressures to a minimum, nominally less than 6.9E6 Pa (1,000 psi). There is also the question of whether shale formations can retain pressure for extended periods of time or if leak-off from the reservoir will hamper energy storage efforts. To answer these questions, we used our dual-porosity reservoir model to quantify maximum flow rates, pressures during injection and production, and leak-off from the reservoir. Our model simulates a constant pressure boundary by allowing leak-off from the SRV to a large volume of unstimulated matrix outside of the SRV. No leak-off was observed beyond the boundary of the unstimulated matrix in our simulated cycles. Details of the model are found in Augustine et al. (2021a) and outlined in the STAR Methods section.

We developed an idealized energy storage cycle model consisting of four phases— an injection phase during which natural gas is injected into the reservoir to store energy, a storage phase during which the well is shut in, a production phase during which natural gas is produced from the reservoir to generate electricity, and a recovery period during which the well is shut in. After the recovery period, the storage cycle is repeated starting with another injection phase. Figure 4 shows these cycles for the diurnal model. For simplicity of presentation, the idealized cycle assumes that each of these phases are equal in time duration. This may not be the most efficient way to cycle the reservoir as slower compression rates and longer times may be more adiabatic and thus more efficient, nor is it likely an operational cycle for a real system striving to optimize energy supply and demand cycles. We considered two time frames for energy storage. The first is a short-term, diurnal energy storage cycle where energy is stored and released on a daily basis. This cycle takes 24 h to complete, with each phase lasting six hours. The second is a long-term, seasonal energy storage cycle where excess energy generated in one season is stored long-term for use in another season. Each phase of the long-term cycle lasts 90 days so that the cycle takes 360 days, or roughly a year, to complete. These are arbitrary storage cycles chosen for convenience. Actual storage and production durations will be market-driven.

First, we developed a conceptual model of a hydraulically fractured reservoir using data from literature when possible. Next, we validated the model by minimizing numerical effects and comparing the results

to analytical solutions. We performed sensitivity analyses to determine the major factors controlling reservoir performance. Finally, we used the validated model to simulate the energy storage cycle for three major shale gas formations—the Marcellus, the Haynesville, and the Barnett (see Figure 2). The pressure and flow data were then input into a wellbore and surface plant model to calculate round-trip efficiencies.

Reservoir model development

Numerical reservoir models of a multistage, hydraulically fractured, horizontal gas well were built using the commercial software CMG-GEM, which is an equation-of-state (EoS) reservoir simulator for compositional, chemical, and unconventional reservoir modeling(Computer Modeling Group, 2017). This model can accommodate dry gas, wet gas, and liquid systems as a multicomponent, dual-porosity reservoir.

The ability to predict and control injection and production of natural gas into and from a hydraulically fractured shale reservoir is one of the most important and challenging aspects of the REFRAES concept. Injectivity and productivity are properties of the reservoir, and not all reservoirs will be good candidates for energy storage with compressed natural gas. The goals of reservoir modeling in this study were to 1) identify reservoir parameters that control gas injectivity, storativity, and productivity, and 2) determine the feasibility of energy storage in shale reservoirs.

Reservoir model results

Preliminary modeling runs taught us several things about reservoir behavior during cyclic energy storage operations. Our early focus was on short-term or diurnal energy storage (shown in Figure 4), but the long-term model (not shown) gave similar trends but with longer timelines. A diurnal energy storage cycle was modeled as follows:

- Six hours of natural gas injection (electricity storage)
- Six hours of shut-in (storage period)
- Six hours of natural gas production (electricity generation)
- Six hours of shut-in (recovery period)

The goal for diurnal energy storage operation was to achieve steady-state operation of the reservoir cycles over time. Objectives included:

- Maximize natural gas flow rate (power generation capacity)
- Minimize the wellhead pressure difference between injection and production (round-trip efficiency)
- Achieve net-zero cumulative injection of natural gas over time (no leakage from reservoir, eliminate need for purchasing natural gas)

We implemented model runs as follows. First, the model was initialized at reservoir pressure and temperature. Next, natural gas was produced for one year to represent partial reservoir depletion. After a shut-in period (usually 45 days), the diurnal energy storage cycles started by adjusting the well's flowing bottom-hole pressure (BHP). Flowing BHP was increased to a pre-determined level (above average reservoir pressure) and held constant during the injection phase, and it was decreased to a pre-determined level (below average reservoir pressure) and held constant during the production phase. The cycles were repeated for anywhere from one day to hundreds of days.

We quickly observed that reservoir behavior during cycling was controlled mainly by differences between flowing pressures and average reservoir pressure, which is called pressure drive. We could achieve sustainable cyclic operation—loosely defined as net-zero natural gas injection over time—by setting the injection and production BHPs to the same value above and below (respectively) average reservoir pressure. For example, if average reservoir pressure was 2.8E7 Pa (4,000 psi), then steady-state operations could be achieved by setting the injection and production BHP to 3.1E7 Pa (4,500 psi) and 2.4E7 Pa (3,500 psi), (4,000 psi $\pm$500 psi pressure drive), respectively. Figure 4 shows the results of the model which match similar cyclic trends seen in porous media compressed-air energy storage models (Gabrielli et al., 2020;

Kushnir et al., 2008; Oldenburg and Pan, 2013). The following broad observations in each of the four phases are discussed below.

1) Injection:

BHP rises quickly to a preset level until gas injection is halted.

The gas injection rate initially spikes but decreases with time over the course of a cycle as pressure in the reservoir increases.

2) Injection shut-in:

BHP decreases exponentially, asymptotically approaching a steady-state value near the original BHP. This is due to injected gas and increased pressure near the wellbore dissipating into the formation.

3) Production:

BHP decreases quickly to a preset level until gas production is halted. Like with injection, the initial gas flow rate is high and then decreases as the pressure in the reservoir decreases.

4) Production shut-in:

A similar but opposite response as injection shut-in; BHP increases exponentially, asymptotically approaching a steady-state value near the original BHP. This is due to gas coming from the formation toward the wellbore in response to the pressure sink left from the production phase.

Preliminary modeling also showed that the BHP returns to near the pre-injection or pre-production reservoir pressure within the same length of time as the injection or production event. This demonstrates that the hydraulically fractured shale reservoir does not actually "hold pressure" after small volumes of gas are injected. The natural gas moves farther out into the fractures and rock matrix as the BHP pressure equilibrates to average reservoir pressure. However, the model does show that this natural gas can be produced back, so that over the long-term, the pressure in the reservoir can be managed and maintained at a desired operation point. The energy storage cycle can then be designed and optimized to operate around average reservoir pressure. We measured reservoir performance by its injectivity and productivity indices, which quantify how high a flow rate can be achieved for a given pressure drive. The higher this value, the better-suited is the reservoir for energy storage. Sensitivity analysis showed that reservoir-effective permeability and matrix permeability control flow rate for a given pressure drive, with higher permeabilities giving higher flow rates. However, flow rates varied by less than an order of magnitude over these ranges. This indicates that if feasible, energy storage in shale could be conducted over a wide range of formation permeabilities.

Using the aforementioned outlined methodology , we simulated short- and long-term storage at depleted reservoir pressures equal to 1.4E7 Pa (2,000 psi) using reservoir data from the Marcellus, Haynesville, and Barnett unconventional gas fields (Table 1). Matrix and fracture storage and flow characteristics are represented in dual-porosity models using parameters such as net pay and effective SRV system permeability. Some rock intervals within the total SRV vertical thickness are not productive and these unproductive intervals are excluded from the models. Net pay represents the cumulative vertical thickness of productive intervals within the SRV, and effective SRV system permeability represents the permeability of the matrix-fracture system.

The Marcellus model resulted in average gas flow rates of 1.5 MMscfd for the short-term storage cycle and 0.7 MMscfd for the long-term storage cycle (Table 2). The Barnett results were similar, with flow rates of 1.1 MMscfd and 0.6 MMscfd for the short- and long-term storage cycles, respectively. These results assume 10–12 fracture stages, which was typical for wells drilled around 2011, when the data were collected (Dong et al., 2014). The trend has been to complete increasingly longer horizontal wells (~4800 meters long) with 160–480 hydraulic fracture stages (Siddhamshetty et al., 2019). Because flow rates scale linearly

Table 1. Low, middle, and high reservoir parameter values used in parametric analysis of Barnett, Marcellus, and Haynesville shale plays.

	Barnett – 10 fractures			Marcellus – 12 fractures			Haynesville – 13 fractures		
	Low	Mid	High	Low	Mid	High	Low	Mid	High
Net pay (ft)	100	200	600	45	120	384	100	200	300
Pressure (psi)	1,000	2,000	3,000	1,000	2,000	3,000	1,000	2,000	3,000
Effective SRV system permeability (mD)	7E–5	5E–4	5E–3	2E–4	3E–4	9E–4	5E–4	3E–2	4E–1
Porosity (%)	0.4	2.7	5.0	3	6	13	8	12.6	14
Water saturation (%)	43	34	25	53	26	6	41	28.5	16

with the number of fracture stages, it is reasonable to assume that modern wells could sustain flow rates of ~5 MMscfd for short-term storage cycles and ~2 MMscfd for long-term storage cycles. The gas flow rates for the Haynesville model results were about a factor of 10 lower. The Haynesville reservoir is initially geopressured and it experiences compaction during depletion, which reduces reservoir permeability (Okouma et al., 2011).

Reservoir modeling conclusions

Results from the conceptual model showed that the reservoir does not maintain the bottomhole pressure developed during injection, or "hold pressure" over the duration of the storage period. Instead, the bottomhole pressure declines rapidly and equilibrates close to the initial reservoir pressure within hours for the diurnal cycle and within weeks for the seasonal cycle (not shown). However, the cycle can be operated in a steady-state fashion where natural gas injection over time is roughly net-zero by maintaining the injection- and production-well bottomhole pressures at equal distances from the initial or resting reservoir pressure. Although the reservoir does not hold pressure, reinjection does maintain a constant reservoir pressure over time so that energy storage cycles can be repeated many times without depleting reservoir pressure. The results also showed that flow rates increase linearly as the difference between the initial and flowing bottomhole pressures, or pressure drive, increases, and vice versa. Thus, the key to making energy storage in shale wells feasible is to identify reservoirs with sufficient flow rates at acceptable pressure losses for energy storage. Although outside the scope of this paper, our model could be used for this purpose using existing well data.

The flow rates from the model results for the Marcellus and Barnett shale gas wells are within the target range of 1–10 MMscfd from preliminary surface plant modeling at pressure drives of +/− 3.4E6 Pa (+/−500 psi). The model results indicate that energy storage in horizontal, multi-zonal hydraulically fractured shale gas wells is feasible. Based on these reservoir modeling results, we modeled the wellbore and surface equipment assuming flow rates of several MMscfd.

Table 2. Low, average, and high natural gas flow rates for short- and long-term storage cycles from parametric analysis using parameters.

Oil/gas field	Rate per typical well (low-average-high): Short-term storage (mmscf/day)	Rate per typical well (low-average-high): Long-term storage (mmscf/day)
Marcellus injection rate	0.7–1.6–1.9	0.1–0.6–1.5
Marcellus production rate	0.5–1.5–1.8	0.1–0.7–1.6
Haynesville injection rate	0.05–0.08–0.12	0.03–0.08–0.12
Haynesville production rate	0.04–0.08–0.11	0.02–0.07–0.11
Barnett injection rate	0.5–1.2–1.4	0.0–0.5–1.2
Barnett production rate	0.5–1.1–1.3	0.1–0.6–1.2

Short-term storage: 6 h injection, 6 h shut-in, 6 h production, 6 h shut-in; long-term storage: 90 days injection, 90 days shut-in, 90 days production, 90 days shut-in.
see Table 1

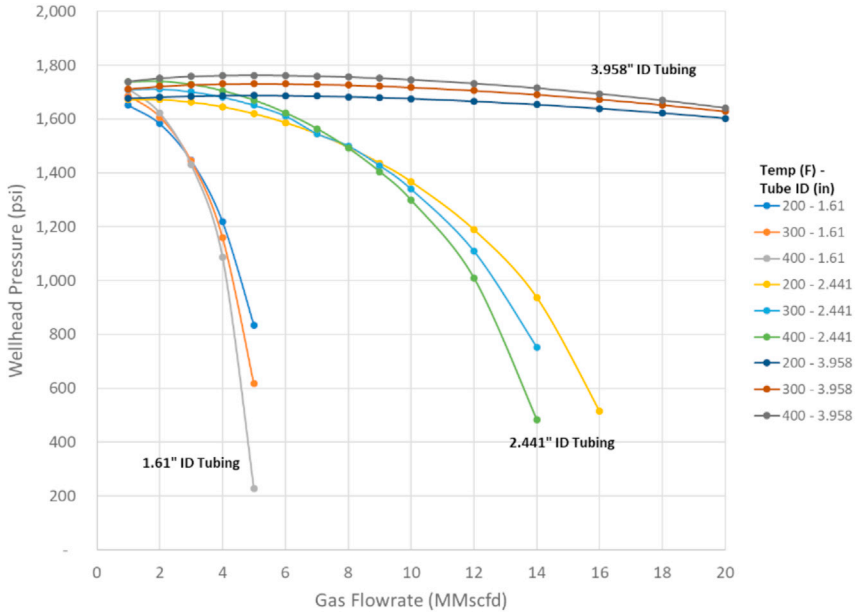

Figure 5. Wellhead pressure during production of natural gas vs. flow, bottomhole temperature, and tubing ID for bottomhole pressure = 2,000 psi and depth = 8,500 ft

Wellbore model

Pressure and heat losses from the natural gas during injection, storage, and production lower the round-trip efficiency of the REFRAES energy storage cycle. Natural gas is normally produced through tubing installed in the well after it is cased and completed. The tubing inner diameter varies based on production flow rates and is limited by the diameter of the production casing, which can vary based on the well completion. During injection and production, friction within the wellbore tubing results in pressure losses. Higher flow velocity results in greater pressure losses. Additionally, pressure changes with depth due to gravity effects. Heat loss through the tubing into the formation can be significant as well, especially for low flow rates. CMG software does have the ability to model flow in wellbores, but because we decided to model the reservoir with a single fracture for computational efficiency, the flow rates are for a single fracture and are much lower than they would be for the full well.

Instead, we developed an Excel-based model for pressure and temperature losses in the wellbore (Figure 3). We used the analytical solution developed by Hagoort (2005) for predicting wellbore temperatures and pressures in gas production wells. The solution is based on the extended Bernoulli equation and the steady-state energy balance of flow through the wellbore and accounts for the effects of gravity, friction, and wellbore heat losses. By accounting for heat losses, the Hagoort analytical solution is able to calculate both the pressure and the temperature at the wellhead given the bottomhole pressure and temperature. The analytical model is solved via an iterative process until given tolerance is achieved. The model can be made more accurate by dividing the wellbore into sections and solving them sequentially, with the outputs from one section becoming the inputs for the next section. We divided the well into 10 segments during calculations to increase accuracy.

The Hagoort analytical model was developed specifically for production. We adapted it to model well injection and validated the model by comparing the results to those for the popular Cullender-Smith analytical solution for calculating bottomhole pressure, ensuring that the inlet and outlet temperatures from the well were identical between the models (i.e., both models had the same temperature profile because Cullender-Smith does not implicitly account for heat losses). Implementing the model in Excel allowed us to isolate and analyze the magnitude and sources of temperature and pressure losses in the wellbore separate from the influence of the reservoir model results.

Figures 5 and 6 show the wellhead pressure and temperature, respectively, during natural gas production as a function of flow rate, bottomhole temperature, and tubing inner diameter (ID). We assumed that a

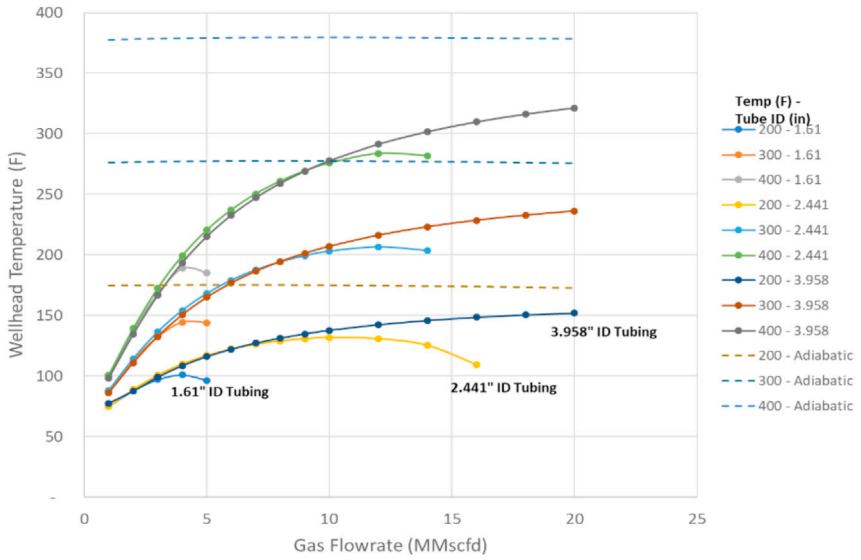

Figure 6. Wellhead temperature during production of natural gas vs. flow, bottomhole temperature, and tubing ID for bottomhole pressure = 2,000 psi and depth = 8,500 ft

surface formation temperature of 10°C (50 °F) and all other unspecified parameters use the same values presented in the example calculations in Hagoort (2005). The figures demonstrate how gravity, friction, and heat loss affect the wellhead temperature and pressure during production. As flow rate increases, the total thermal energy in the gas compared to the heat lost to the wellbore increases, so that it maintains a higher temperature during production (Figure 6). However, higher flow rates lead to greater pressure loss due to friction (Figure 5). Smaller diameter tubing results in higher velocities and greater friction losses for a given flow rate. At some point, the pressure losses due to friction become high enough that Joule–Thomson expansion of the gas causes the temperature to decrease with flow rate (Figure 6). At even higher flow rates, the pressure losses are high enough that the wellhead pressure equals atmospheric pressure, and the flow rate cannot be increased further. The results indicate that tubing ID can place practical restrictions on the flow rates that can be achieved in production gas wells during REFRAES operations.

Figures 7 and 8 show the wellhead pressure and bottomhole temperature, respectively, during natural gas injection as a function of flow rate, injection and bottomhole temperature, and tubing ID. The natural gas should be elevated in temperature from the compression stage prior to injection. For convenience, we assumed that the injection temperature is the same as the bottomhole temperature. During injection, hydrostatic pressure increases the pressure of the gas as it moves down the hole, while friction losses decrease the pressure. This explains why at low flow rates the wellhead pressure is lower than the bottomhole pressure, and as flow rate increases the wellhead pressure increases to counteract increasing friction losses. Smaller diameter tubing results in higher velocities and greater friction losses for a given flow rate. The results again indicate that tubing ID can place practical restrictions on the flow rates that can be achieved in injection gas wells during REFRAES operations. The bottomhole temperature as a function of gas flow rate goes through a minimum (Figure 8). This is because the formation at the surface is lower in temperature than the injected gas, so the gas loses thermal energy to the wellbore during injection. As depth increases, so does temperature. At some point in the wellbore, the formation temperature becomes higher than the temperature of the gas in the wellbore and the gas gains thermal energy. The minimum is caused by the interplay of thermal losses and gains as a function of flow rate as the gas travels down the well.

One of the advantages of REFRAES is its potential to store thermal energy from compression in the reservoir, which increases the round-trip efficiency of the process. However, Figures 6 and 8 show that heat losses from the wellbore during injection and especially production threaten to negate this advantage. Low temperatures at the production wellhead result in less power generation from the expander. One potential solution is the use of insulated wellbore tubing to minimize thermal losses (Vallourec, 2014). Natural gas is

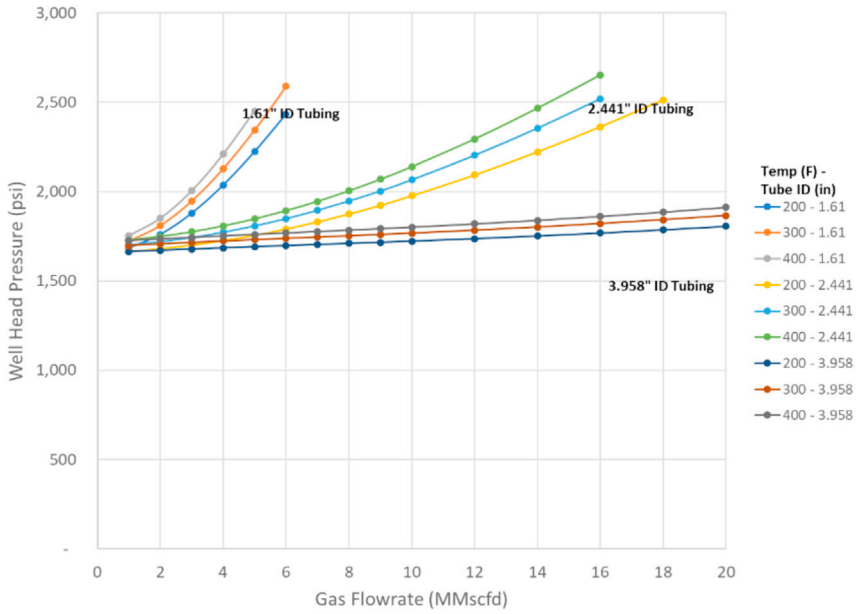

Figure 7. Wellhead pressure during injection of natural gas vs. flow rate, wellhead temperature, and tubing ID for bottomhole pressure = 2,000 psi and depth = 8,500 ft. Assumed that injection temperature is identical to reservoir temperature

usually produced through tubing that separates the produced fluid from the permanent well casing. Installing or replacing tubing in the well is a common oil and gas field practice that can be completed in hours to days. Although not studied here, it should be noted that the well casing itself might be used for REFRAES to greatly increase the flow rate. Figure 9 shows the wellhead temperature during production as a function of flow, bottomhole temperature (BHT), and tubing ID for an insulated well, assuming an overall wellbore heat-transfer coefficient of 10% of that of uninsulated (bare) tubing. The temperature profiles are much closer to the adiabatic (zero heat loss) production wellhead temperatures, even at lower flow rates. The pressure profiles for the insulated tubing are similar to those for bare tubing. Heat losses through

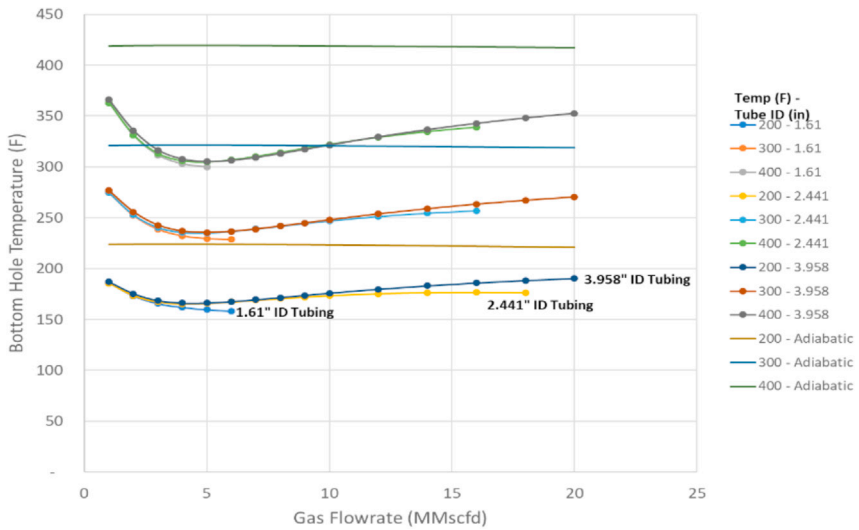

Figure 8. Bottom hole temperature during injection of natural gas vs. flow, wellhead temperature, and tubing ID for bottomhole pressure = 2,000 psi and depth = 8,500 ft. Assumed that injection temperature is identical to reservoir temperature

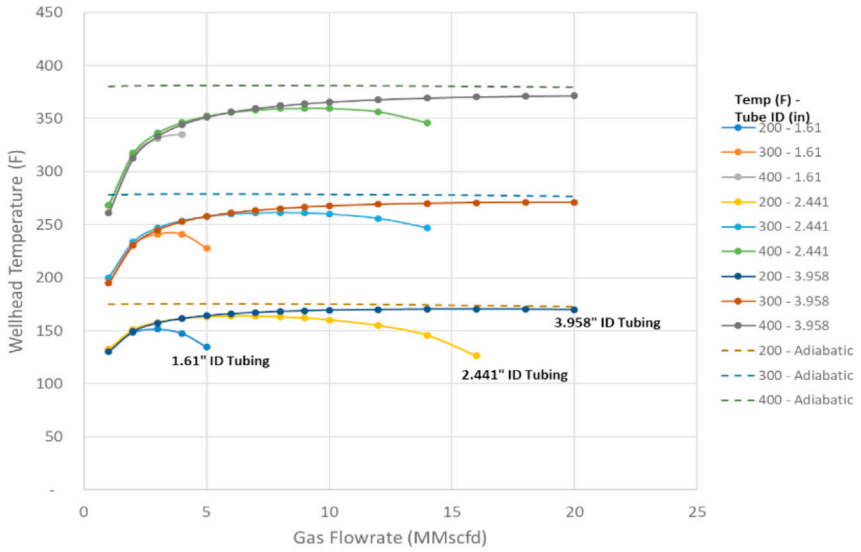

Figure 9. Wellhead temperature of insulated well during production of natural gas vs. flow rate, bottom hole temperature, and tubing ID for bottomhole pressure = 2,000 psi and depth = 8,500 ft

tubing appear to have the potential to decrease REFRAES performance and need to be studied in greater detail.

Surface plant model

Sections 2 and 3 describe the reservoir model and wellbore model, respectively. The last piece in the REFRAES system is the surface plant model (Figure 3). Because the REFRAES concept uses relatively low compression and expansion ratios and uses the subsurface to store and manage thermal energy, the surface plant does not require inter- or post-coolers for the compressor, pre-heaters or gas combustion prior to the expander, or surface thermal energy storage equipment. The REFRAES surface plant model consists of only two components: 1) an electricity-powered compressor for gas injection and 2) an expander to produce electricity from the produced gas.

The work for both the natural gas compressor (W_{comp}) and expander (W_{exp}) with given inlet temperatures (T_{in}) and pressures (P_{in}) and known outlet pressures (P_{out}) can be described by the same equation:

$$W = \Delta H = \frac{\Delta H_{isentropic}}{\eta} = \frac{H_{in}(S_{in}, P_{in}) - H_{out}(S_{in}, P_{out})}{\eta}$$

where ΔH is the actual change in entropy of the natural gas, $\Delta H_{isentropic}$ is the isentropic change in enthalpy of the natural gas, S_{in} is the entropy of the inlet natural gas, and η is the efficiency of the machine (compressor or expander). Once the actual enthalpy change is known, the outlet temperature can be determined from the enthalpy and pressure at the outlet.

We used the REFPROP (Lemmon et al., 2018) add-in in Microsoft Excel® software to calculate natural gas thermodynamic properties. REFPROP calculates the thermodynamic and transport properties of industrially important fluids and their mixtures. We used the "Natural Gas" (NGMIXTURE.DAT) mixture fluid in our calculations. We assumed an efficiency of 85% for both the compressor and the expander based on conversations with original equipment manufacturers.

Limitations on operating pressures and temperatures for the compressor and expander are determined by the reservoir pressure and temperature, temperature limitations of the well, and the natural gas gathering lines that we intend to use as a source and sink for natural gas. Natural gas line gathering pressures vary among locations but are generally in the range of 6.9E5–3.4E6 Pa (100–500 psi). The ability to buy back natural gas from the gathering lines— to use in gas lift operations, for example—is common in the field. Reservoir pressures also vary greatly, even over the life of a single well as it is depleted. The temperature

Table 3. Temperature and pressure limitations in REFRAES process.

Parameter	Controlling factor(s)	Assumed range/value
Compressor inlet temperature	Natural gas collection line temperature	10°C (50 °F)
Compressor inlet pressure	Natural gas collection line pressure	100–500 psi
Compressor outlet temperature	Well temperature limitations	<204°C (400 °F)
Compressor outlet pressure	Reservoir pressure and depth	<3,000 psi
Expander inlet temperature	Well temperature limitations	<204°C (400 °F)
Expander inlet pressure	Reservoir pressure and depth	<3,000 psi
Expander outlet temperature	Condensation in exhaust, natural gas collection line temperature limitations	>10°C (50 °F)
Expander outlet pressure	Natural gas collection line pressure	100–500 psi

limit out of the expander depends on the type of expander used and by the potential for liquids to condense out of the gas at low temperatures. Table 3 summarizes the temperature and pressure ranges we assumed for this study.

We modeled the compressor work requirements and expander work output over the ranges in Table 3. Figure 10 shows the compressor power requirements on a per MMscfd of natural gas flow rate basis and the compressor outlet temperature as a function of inlet and outlet pressure. As one would expect, power requirements increase with pressure and compression ratio. However, the temperature outlet remains below 204°C (400 °F) for most of the combinations.

Figures 11 and 12 show expander power output on a per MMscfd of natural gas flow rate basis and the expander outlet temperature as a function of inlet and outlet pressure. Like with the compressor, power increases with pressure and expansion ratio. However, owing to the Joule–Thomson effect, natural gas cools as it goes through the expander. Figure 11 shows that for an inlet temperature of 93°C (200 °F), the exit temperature falls below 10°C (50 °F) (the assumed temperature from the natural gas gathering lines) for most of the inlet/outlet pressure combinations. Figure 12 shows that if the inlet to the expander can be increased to 149°C (300 °F), the outlet temperature is significantly higher and less likely to create dew point issues in or downstream from the expander.

Integrated REFRAES cycle

We now combine the results of reservoir, wellbore, and surface plant models to integrate the inputs and outputs from the models to develop a complete model of REFRAES system. An integrated REFRAES cycle starts with running the compressor model to determine the compressor outlet/well inlet conditions. Next, the wellbore injection model determines the conditions at the bottom of the wellbore before entering the reservoir.

The results from each model provide the inputs for the next model. The reservoir model tells us what production flow rate and bottomhole pressure to use as inputs to the production wellbore model. Finally, the expander model calculates power output and gas conditions before being returned to the sales line. We ran the models sequentially to calculate the complete results for the integrated REFRAES cycle. We assume a constant flow rate equal to the average well flow rate over the injection or production period. We present a base case scenario and an informed favorable scenario based on an extensive parametric analyses study.

REFRAES base case scenario

Figure 13 shows the conditions we chose for the REFRAES base case scenario. User-defined inputs, consisting of the compressor inlet conditions, wellbore attributes, and reservoir operating conditions, are shown in italics. The inputs for the flow rate as a function of the pressure difference between the bottomhole conditions and the reservoir average pressure ("Reservoir/BH ΔP") is not strictly from reservoir models but is approximate and is informed by results from reservoir model results. The base case assumes a reservoir with a resting bottom hole pressure of 1.0E7 Pa (1,500 psi) at 121°C (250 °F) capable of injection/production flow rates of 3 MMscfd from a 1.7E6 Pa (250 psi) pressure drive, giving a total difference of (3.4E6 Pa (500 psi) between the injection and production phase bottomhole pressures. The wellbore model results show the

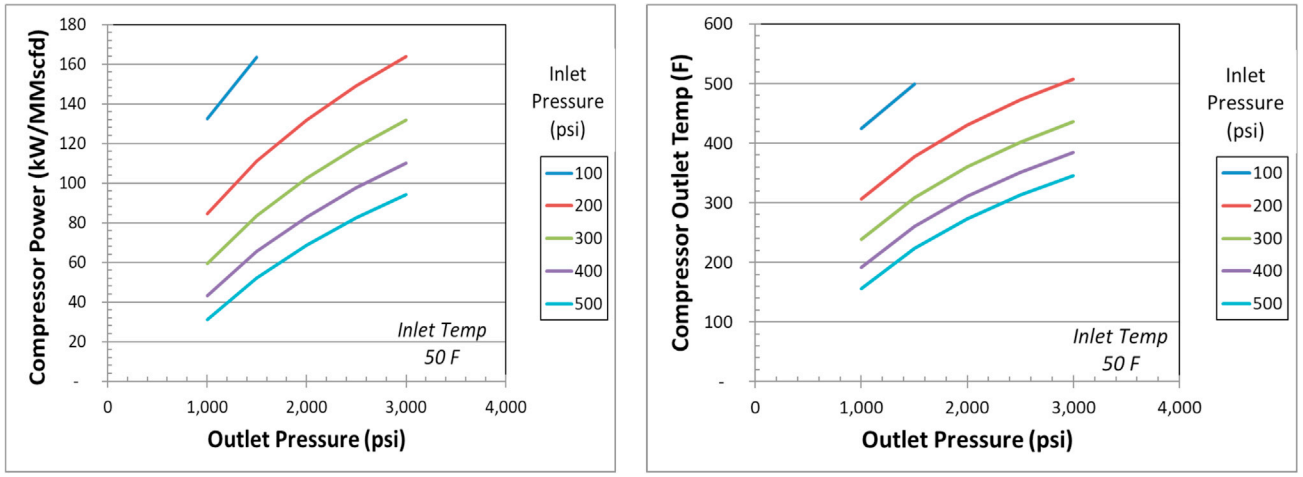

Figure 10. Compressor power requirements and outlet temperature as a function of inlet and outlet pressure. Compressor inlet temperature is 50 °F. Compressor efficiency is assumed to be 85%

pressure difference between injection and production at the wellhead is 3.8E6 Pa (550 psi), slightly larger than the bottomhole difference. The wellbore is assumed to be 90% insulated, which for this study is interpreted as meaning the overall heat-transfer coefficient for the wellbore is 90% less than in the uninsulated scenario. Even with this insulation, the temperature in the injection well still drops from 177°C (350 °F) coming out of the compressor to 134°C (274 °F) at the bottomhole before being injected into the reservoir. The model assumes that the bottomhole production temperature is the same as the original reservoir temperature 121°C (250 °F). This implicitly assumes that injection temperatures have no impact on production temperatures and the reservoir temperature dictates the production temperature. The natural gas temperature after expansion is 3.3°C (38 °F), just above freezing. This could cause issues in the expander owing to the potential formation of ice droplets. The cycle requires 257 kW during injection and produces 124 kW during production for a net round-trip efficiency (RTE) of 48.5%

Parametric analyses

With a view to increasing the RTE we performed parametric analyses to illustrate how input parameters affect performance. All of the user-defined inputs identified in Figure 13, with the exception of the compressor inlet temperature, were individually varied over a range of values (production BHT is

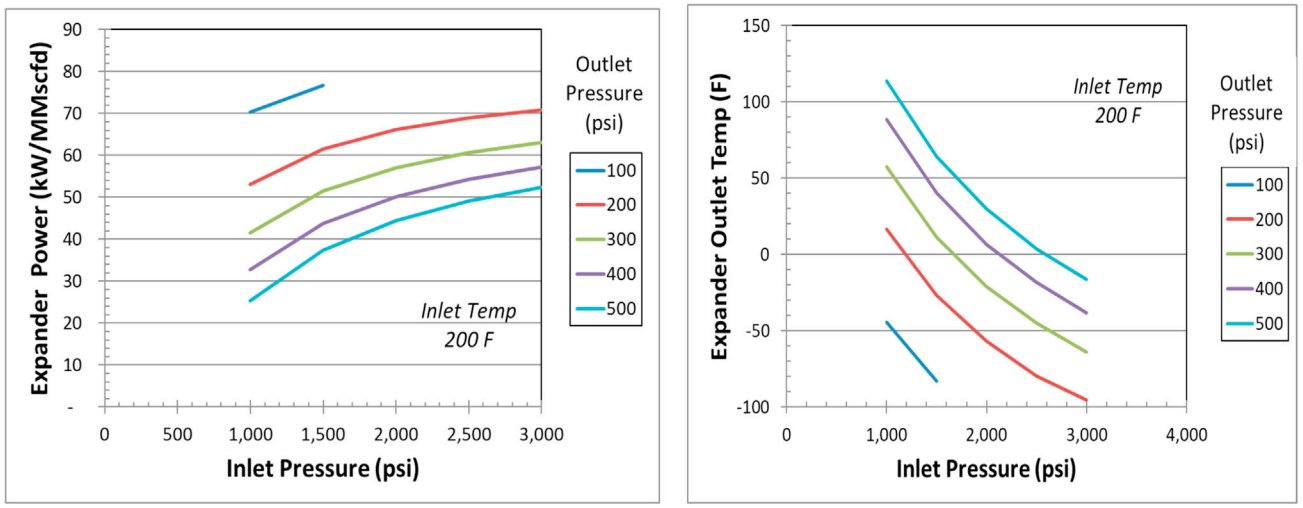

Figure 11. Expander power output and outlet temperature as a function of inlet and outlet pressure. Expander inlet temperature is 200 °F. Expander efficiency is assumed to be 85%

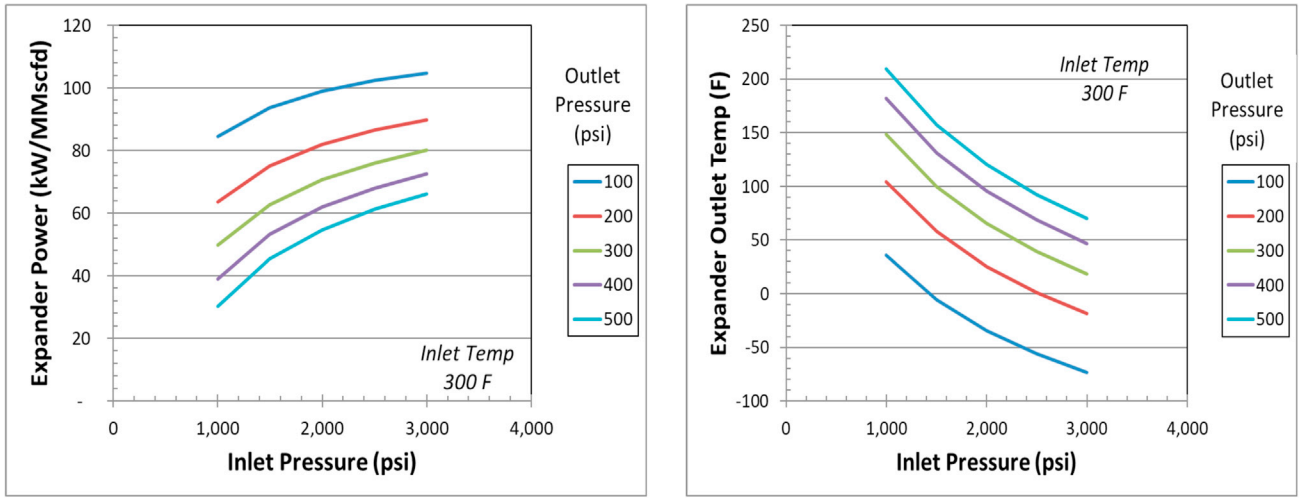

Figure 12. Expander power output and outlet temperature as a function of inlet and outlet pressure. Expander inlet temperature is 300 °F. Expander efficiency is assumed to be 85%

considered in a later parametric analysis). For each run, we report the results for the key output parameters of compressor power in, expander power out, and expander outlet temperature.

Figures 14 and 15 show the results of these analyses. The RTE varies from 23% to 57%, with most cases resulting in an RTE of 45%–50%. For some cases, the selected flow rate was larger than what is physically possible for the given wellbore diameter and bottomhole pressure. A consistent result across cases is a low temperature at the expander outlet. Outlet temperatures below 0°C (32 °F) could cause water droplets in the produced gas to freeze during expansion, which could complicate or prevent the use of some types of expanders. We set a target lower limit of 10°C (50 °F) for the expander outlet temperature to provide a safety margin for operating equipment. Figures 14 and 15 show that the outlet temperature is below 10°C (50 °F) for the majority of the cases studied and is below 0°C (32 °F) for almost a third of the cases. The natural gas cools as it expands in the expander. Its outlet temperature from the expander is a function of its inlet temperature and the expansion ratio. Parameters that increase the inlet temperature to the expander, such as minimizing heat loss in the wellbore, increasing the flow rate (which minimizes heat loss in the wellbore relative to total thermal energy content), and increasing the well BHT, all work to increase the outlet temperature from the expander. Parameters that decrease the expander inlet pressure (decreasing reservoir pressure, increasing reservoir pressure losses) or increase the outlet pressure (increasing the natural gas collection line pressure) also increase the expander outlet temperature.

Compressor Inlet			
Flow (MMScfd)	Power In (kW)	Temp (F)	Pressure (psi)
3	257	*50*	*250*

Expander Outlet			
Temp (F)	Pressure (psi)	Power Out (kW)	RTE (%)
36	*250*	124	48.1%

			Wellbore			
Injection WH	350	1,588	ID (in)	201	1,035	Production WH
			2.441			
			Insulation			
			90%			
Injection BH	316	*1,750*		*250*	*1,250*	Production BH

	Reservoir/BH ΔP (psi)	
1,500	*250*	*250*
	Reservoir Conditions	

Figure 13. REFRAES base case scenario for round-trip efficiency calculations. User-defined inputs for the base case are shown in italics

Heat loss in wellbore

% Insulated	Compressor Power	Expander Power	Expander Temp Out	RTE
%	*kW*	*kW*	*°F*	*%*
0%	251	98	-50	38.9%
50%	253	107	-20	42.2%
90%	257	124	36	48.1%
95%	258	127	46	49.2%
99%	258	129	56	50.1%

Reservoir Pressure

P_b	Compressor Power	Expander Power	Expander Temp Out	RTE
psi	*kW*	*kW*	*°F*	*%*
1000	203	78	103	38.4%
1500	257	124	36	48.1%
2000	302	145	-3	48.1%
2500	340	158	-31	46.4%
3000	374	166	-52	44.5%

Reservoir Pressure Losses (ΔP Injection vs. Production)

ΔP	Compressor Power	Expander Power	Expander Temp Out	RTE
psi	*kW*	*kW*	*°F*	*%*
125	245	130	24	53.2%
250	257	124	36	48.1%
500	280	106	63	37.8%

Flow rate in wellbore

Flow rate	Compressor Power	Expander Power	Expander Temp Out	RTE
MMscf/d	*kW*	*kW*	*°F*	*%*
1	84	39	-1	46.3%
3	257	124	36	48.1%
5	442	198	53	44.7%
10	n/a - exceeds maximum flow rate for well			

Figure 14. Results of parametric analyses for changes in heat loss in the wellbore, reservoir pressure, reservoir pressure losses, and flow rate in the wellbore. The first column shows the parameter being varied. The remaining columns show results for the compressor power, expander power, temperature out of the expander, and the round-trip efficiency. All other parameters are set to the values in the base case scenario (Figure 13)

One of the major findings of the parametric analyses is that heat loss in the wellbore is low enough to not require insulated tubing to prevent dew point damage to the expander equipment in some situations. Although without insulation, the REFRAES cycle only achieves a 40% RTE. Insulated tubing increases cycle RTE and increases the expander outlet temperature and should be considered in REFRAES installations. Increasing reservoir pressure increases total power output but has mixed effects on RTE and decreases the expander outlet temperature. Pressure losses within the reservoir have a noticeable impact on RTE

Tubing Diameter (vs. Flow Rate)

d_h	Flow	Compressor Power	Expander Power	Expander Temp Out	RTE
in	*MMscf/d*	*kW*	*kW*	*°F*	*%*
3.958	1	84	38	-5	46.1%
3.958	3	253	126	30	49.9%
3.958	5	423	214	40	50.6%
3.958	10	858	427	50	49.8%
1.61	1	85	38	2	44.7%
1.61	3	288	65	104	22.6%
1.61	5	n/a - exceeds maximum flow rate for well			
1.61	10	n/a - exceeds maximum flow rate for well			

Reservoir/Production Well BHT

T_b	Compressor Power	Expander Power	Expander Temp Out	RTE
°F	*kW*	*kW*	*°F*	*%*
200	257	112	-2	43.5%
250	257	124	36	48.1%
300	257	135	74	52.6%
350	257	147	113	57.0%

Natural Gas Collection Line Pressure

P_{in}	Compressor Power	Expander Power	Expander Temp Out	RTE
psi	*kW*	*kW*	*°F*	*%*
100	440	184	-47	41.8%
300	224	110	54	49.0%
500	139	69	110	49.3%

Figure 15. Results of parametric analyses for changes in tubing diameter (vs flow rate), reservoir/production well BHT, and natural gas collection line pressure. The first column(s) show the parameter being varied. The remaining columns show results for the compressor power, expander power, temperature out of the expander, and the round-trip efficiency. All other parameters are set to the values in the base case scenario (Figure 13)

and should be minimized. Higher flow rates in the wellbore are desirable for improved power output, expander outlet temperature, and RTE, as long as the wellbore tubing diameter is large enough to handle the flow rate. Even large diameter 10 cm (3.958″) ID tubing begins to show a decrease in RTE going from 5 to 10 MMscfd flow rates. Wells with small diameter 4 cm (1.61″) ID tubing are only suitable for low flow rates, indicating that well casing and tubing diameter are important screening criteria for candidate wells.

Increases to the production well BHT has positive benefits for power output, expander outlet temperature, and RTE. The injected natural gas will alter the temperature in the reservoir so that, with time, it will approach the BHT of the injected gas. Additional modeling is needed to determine how long it would take for injection to impact production temperature. The major results from this study show that minimizing heat losses from the wellbore and storing and recovering thermal energy from compression stage in the reservoir have positive impacts on the REFRAES cycle performance leading to RTE of 50%–60%.

REFRAES favorable scenario

The parametric analyses results indicate that the REFRAES cycle can operate over a wide range of conditions and identifies the factors that improve cycle performance. We used these insights to develop a REFRAES favorable scenario that models the REFRAES cycle under conditions that result in improved performance. The following are necessary parameters for improved RTE:

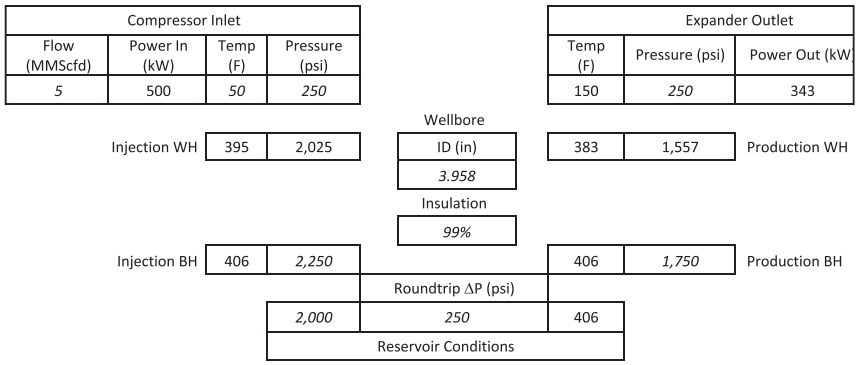

Figure 16. REFRAES favorable scenario for round-trip efficiency. User-defined inputs are shown in italics

- Highly insulated tubing/wellbore
- Reservoir temperature equals injection well BHT (reservoir stores thermal energy)
- Large-diameter tubing (10 cm (4″) diameter)
- High flow rate (5 MMScfd)
- Elevated reservoir pressure
- Minimal pressure losses in reservoir

The actual values used for the input parameters and the model results are shown in Figure 16. This favorable scenario assumes a well with high productivity, capable of producing 5 MMscfd flow rates from a pressure drive between the bottomhole and reservoir of only 1.7E6 Pa (250 psi) (500 psi total pressure swing). The assumption of a highly insulated well results in a BHT of 208°C (406 °F). This thermal energy from compression is stored in the reservoir and is almost entirely returned to the surface. The favorable scenario results in 343 kW of expander output power from a single well and a cycle with almost 70% of RTE. This RTE value approaches that of pumped hydro RTE of 70%–85% (Hydro Review Content Directors, 2021; Luo et al., 2015).

Favorable scenario discussion

The integrated model runs above show that over a wide range of operating conditions, the REFRAES process has the potential to store electricity at round-trip efficiencies that are comparable to conventional CAES projects. A normal or basic well without insulated tubing can likely be used for REFRAES cycles to store energy, but RTE would be relatively low—about 45%–50%—and the expander exit temperature could be low enough to damage equipment. The favorable case, using insulated tubing and a heat-storing reservoir, shows that under the right conditions and some modifications to the wellbore, round-trip efficiencies approaching 70% can be achieved. The lower RTE values are not favorable to diurnal cycles compared with other technologies; however they, are more than adequate for seasonal storage cycles (Albertus et al., 2020).

The runs above are somewhat idealized because they assume constant wellhead pressures and flow rates. Under operating conditions, the pressure and flow rate will vary as the pressure in the reservoir near the wellbore changes with time. However, reservoir model results show that the changes are gradual after initially being established and operational control of pressure and flow should be able to handle the fluctuations. The surface plant model runs aforementioned apply for both short-term and long-term storage.

The parametric analyses show that choosing the operating conditions for a given well will be a balancing act that compromises efficiency for power generation within operational limitations. Higher flow rates lead to greater power generation and can be achieved by increasing the pressure difference (drive) between the bottomhole and the reservoir. However, friction losses also increase with flow rate and eventually cause RTE to decrease with increasing flow rate.

Variable	Description	REFRAES short-term storage (6 hours)		REFRAES long-term storage (90 days)	
n_{RTE}	Round-trip efficiency	40%	70%	40%	70%
P_C	Electricity price during charging ($/MWh)(Schmidt *et al.*, 2019)	0.50			
r	Discount rate (cost of money)(Schmidt *et al.*, 2019)	8%			
T	System lifetime (years)	15			
$O\&M$	Operational and maintenance costs ($/kWh)	0.006			
C_P	Capital cost based on expander power capacity ($/kW)	$3,500	$1,000	$3,500	$1,000
d	Storage duration at rated power (hours)	6		2,160	
n_c	Total number of equivalent full charge-discharge cycles the system performs over time interval t.	365		1	
	Capital costs portion of LCOS ($/MWh)	187	53	187	53
	Electricity cost portion of LCOS ($/MWh)	75	21	75	21
	O&M cost portion of LCOS ($/MWh)	6	6	6	6
	Total Levelized Cost of Storage ($/MWh)	**268**	**80**	**268**	**80**

Figure 17. Input parameters and results for levelized cost of storage

Operating conditions must also be adjusted to prevent exit temperatures near the dew point at the expander outlet that could damage equipment. The integrated cycle runs show the impact that minimizing temperature losses from the natural gas as it flows through the well and maximizing the bottomhole temperature has on the cycle performance. Insulated tubing and the potential for the heated injected gas to raise the reservoir temperature with time are key areas of research that should be explored in the future. Low-temperature solar thermal energy stored on the surface could be used to raise the temperature of the expander gas (Zhang et al., 2013). However, if greenhouse gas emissions are allowed, the natural gas could be heated prior to the expander entrance by drawing off natural gas to burn in in-line heaters. The expander exit temperature would no longer be a limitation and overall power output would be higher as well. Preheating the gas prior to the expander should be considered as an option for early demonstration plants and installations. Future work should include this to quantify the greenhouse gas emissions associated with preheating prior to expansion.

Techno-economic analysis

Techno-economic modeling

Achieving low capital costs ($5,000–35,000/MWh) for energy storage systems is critically important for a viable storage system (Albertus et al., 2020). REFRAES uses existing well and pipeline infrastructure, which reduces risk and capital costs. However, low-cost expander and compressor technology capable of handling the gas/fluid mix likely present during the production phase of the REFRAES cycle is needed to make REFRAES commercially viable. Twin-screw turbines and rotary vane turbines can handle gases, liquids, or multiphase fluids and are versatile enough to handle both compression and expansion cycles.

We developed a rough estimate of the projected capital costs for a 100–1,000 kW system using a vendor assessment of the costs for separate rotary compressor and expander units. We applied cost estimates from a study on a natural gas storage facility (Gülen et al., 2017), resulting in installed capital costs of $1,000–$3,500/kW. The price range depended on project size, RTE (Gülen et al., 2017), and manufacturing cost assumptions. This value could be lower if the expander and compressor are combined into a single unit (Radmax Technologies, 2021). We used these capital cost estimates to calculate the levelized cost of storage (LCOS) using the equation below, adapted from Schmidt et al. (2019) (terms defined in Figure 17).

$$LCOS = \frac{C_P}{n_c d}\left[\sum_{t=1}^{T}\frac{1}{(1+r)^t}\right]^{-1} + \frac{O\&M}{n_c d} + \frac{P_C}{\eta_{RTE}}$$

We calculated the LCOS for short- and long-term storage scenarios using the range of estimated capital costs and RTE from the integrated cycle analysis to bound the answer. Values for the electricity price during

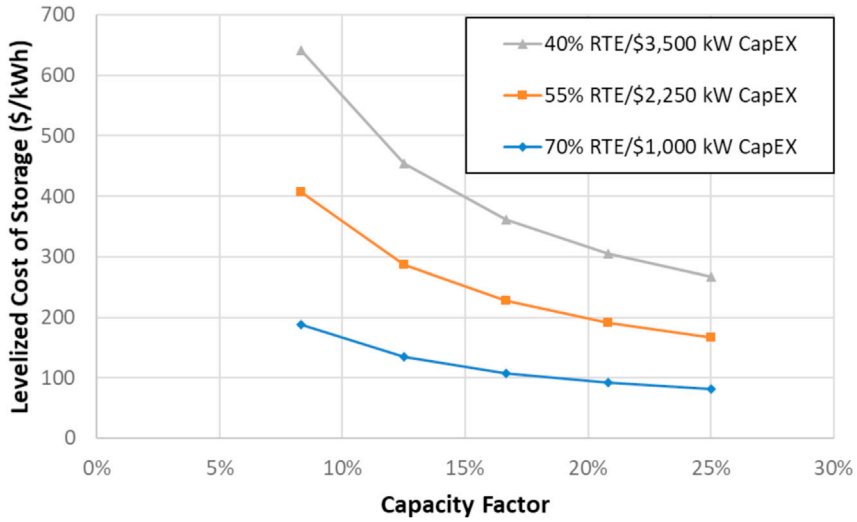

Figure 18. Levelized cost of storage for REFRAES systems as a function of capacity factor. Other parameters for levelized cost of storage calculation are from Figure 17

charging ($/kWh) and the discount rate came from Schmidt et al. (2019). We assumed a project lifetime of 15 years. O&M costs are based on conversations with an OEM of rotary compressor/expander units. Results are shown in Figure 17. For both short- and long-term storage periods the LCOS ranges from roughly 80–270 $/MWh. The LCOS for all cases is dominated by capital costs. The LCOS of the 90-day REFRAES cycle is identical to that for the 6-h cycle because they assume the same 25% capacity factor or ratio of net electricity generation relative to the generation if it operated 100% of the time. Capacity factor is an important parameter when calculating LCOS because it dictates the revenue generated by the project—a higher capacity factor always results in a lower LCOS—but the actual capacity factor for a project depends on the storage needs of the grid. Figure 18 shows the LCOS as a function of capacity factor over the range of RTE and capital costs considered. A capacity factor of 8.3% corresponds to an average of 2 h of storage daily for a diurnal system, or a seasonal storage system that generates electricity 8 h a day for 90 days of the year. Figure 19 shows the sensitivity of LCOS to the electricity price, discount rate, and system lifetime. LCOS is not as sensitive to these factors as it is to RTE, capital costs, and capacity factor. For comparison with other storage technologies, we use the data from Schmidt et al. Traditional CAES can be used for a variety of energy storage applications and grid benefits, but we will focus on energy arbitrage and seasonal storage because these are best suited for the REFRAES technology as presented here (Schmidt et al., 2019). For the energy arbitrage, Schmidt et al. (2019) assume 4 h for discharge duration (d) per cycle and 300 cycles per year (n_c), and for seasonal storage, assume 700 h for discharge duration and 3 cycles per year. Table 4 shows 2018-adjusted US dollars per MWh of stored electricity for the year 2020 for daily energy arbitrage and seasonal storage scenarios for several technologies. For daily energy arbitrage, compressed air, pumped hydro, and lithium ion batteries are the most probable technologies to have the lowest LCOS, with pumped hydro having a mean price of 225 $/MWh. REFRAES is competitive with this value, either matching the value or being significantly lower depending on the RTE and capital costs, as outlined above. The REFRAES costs using the Schmidt energy arbitrage assumptions are higher than in our analysis aforementioned because it assumes a lower capacity factor (13.7% vs. 25%). For seasonal storage, compressed air, pumped hydro, and hydrogen storage are the three leading technologies with compressed air having a mean price of $3,000/MWh. Here, REFRAES outperforms all of these technologies by an order of magnitude lower price per MWh. This is partly because of the high capacity factor of 24% assumed for seasonal storage but mostly because of the assumption that REFRAES uses depleted wells and does not have to pay to develop the storage reservoir. The other technologies investment costs increase significantly with storage duration because they have to pay some cost for storage capacity. For example, Schmidt assumes $80/kWh for pumped hydro storage capacity costs in 2015. For seasonal storage, the long (700 h) discharge duration assumed for seasonal storage translates to $5,600/kW in energy capacity costs, compared with $1,129/kW in power capacity costs (Schmidt et al., 2019). Rather than adjusting the size of the energy storage reservoir to suit the use case, REFRAES changes the power capacity that a given well can support depending on storage duration, with power capacity increasing as storage duration decreases.

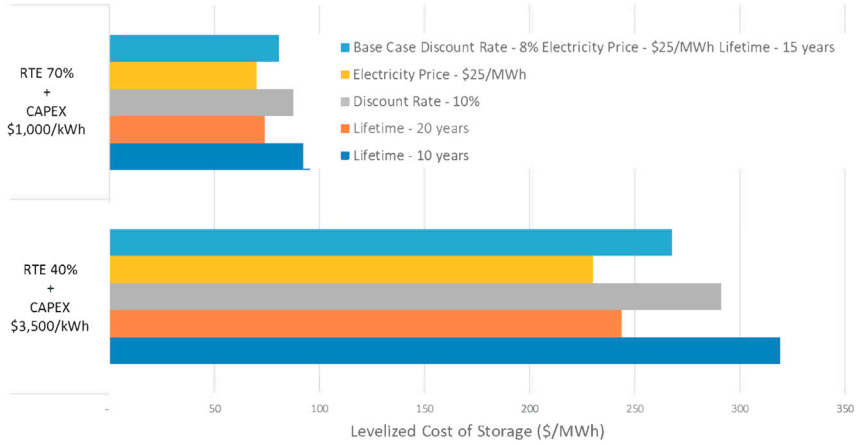

Figure 19. Sensitivity of levelized cost of electricity to electricity price, discount rate, and lifetime

As Table 2 shows, the flow rate, which correlates directly to power capacity, decreases by a factor of 2 or 3 when switching from diurnal to seasonal energy storage, but the storage duration increases by over a factor of 300 (from 6 h to 90 days or 2,160 h). This is a favorable trade-off for REFRAES.

Figure 20 shows average energy storage durations (sec) vs. average system energy capacity (Wh) for several energy storage solutions (adapted from NREL report 2018 PV plus energy storage) (Fu et al., 2018). We note that CAES and pumped hydro have best-in-class total energy capacity and storage duration properties. For a single well converted to REFRAES storage, the discharge time can be varied from hours to many months while the energy capacity is equivalent to mid-size (commercial and industrial) installations of battery technology. However, ganging multiple wells together across drill pads and fields greatly increases the volume of the REFRAES system (assuming each well acts independently) and thus increases the energy capacity. The energy storage capacity of REFRAES is the product of the power capacity and storage duration time. An interesting result from the reservoir modeling is that the relationship between power capacity versus energy storage capacity for REFRAES is highly nonlinear over time. This is due to the slow decline in production flow rate over long periods time. Table 2 shows that when switching from short-term (6 h) to long-term (90 day) storage, the flow rate and hence power output only decreases by half to two-thirds, but the storage duration increases by a factor of 360. This implies that the same well can have a wide range of storage capacity, depending on its storage duration. Increasing storage duration lowers the sustainable power capacity, and this change in power capacity as a function of storage duration ultimately determines the energy storage capacity of a given well.

DISCUSSION

We presented a new technology for large-scale energy storage by compressing natural gas and injecting it into depleted hydraulically fractured wells and releasing the pressurized gas through an expander as a daily energy arbitrage and/or seasonal energy storage solution. We developed three models to account for the

Table 4. Levelized cost of storage for REFRAES and other incumbent technologies in 2018 dollars for daily energy arbitrage and seasonal storage.

	Daily energy arbitrage d = 4 h, n_c = 300 (US, 2018$/MWh)	Seasonal storage d = 700 h, n_c = 3 (US, 2018$/MWh)
REFRAES	124–422	83–276
Pumped hydro	130–320	800–6,400
Compressed air	240–560	800–6,300
Lithium ion	240–680	–
Sodium sulfur	400–760	–
Vanadium redox flow	230–540	10,000–40,000
Hydrogen	–	1,200–5,600

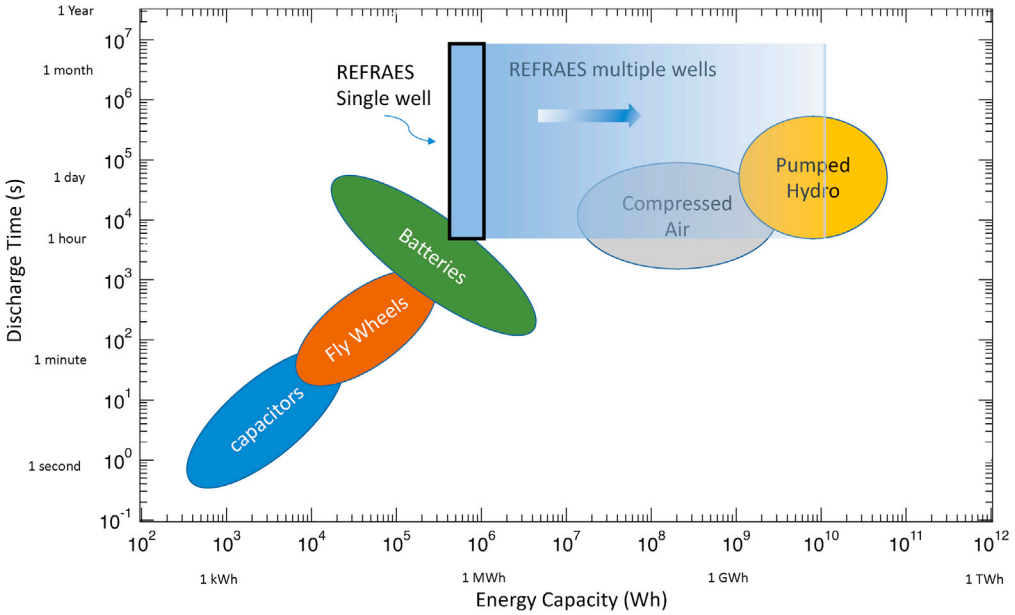

Figure 20. Average energy storage duration vs. system energy capacity (Wh) for several energy storage technologies

thermodynamic state of the gas during its round-trip travel. Firstly, a model which accounts for gas flow within the complex multifaceted reservoir network was developed using commercial petroleum reservoir modeling software. Secondly, a wellbore model accounts for the thermodynamic state of the gas, friction losses, and heat losses during injection and production in the vertical section of the well. Thirdly, a model for compression and expansion surface hardware allows calculation of the RTE for the system. The three models, when coupled together, provide a complete picture of the system which reveals key factors that most influence the RTE.

The models predict an RTE of 70% under favorable conditions, and an RTE of 40%–50% under more conservative assumptions. We estimated installed capital costs to be between $1,000/kW–$3,500/kW. LCOS analysis reveals that REFRAES is commercially competitive compared with incumbent technologies under many circumstances. Assuming a 25% capacity factor, the conservative base case has an estimated LCOS of $275/kWh and the favorable case has an LCOS of $81/kWh. The low LCOS values are due to the reuse of existing infrastructure, including a de-risked reservoir, low capital expenditures for additional needed equipment, and utilizing the geothermal energy of the reservoir to maintain the thermodynamic state of the compressed gas. In all, REFRAES is shown to be a viable technology for energy storage with high RTE, low LCOS, and ability to be expanded in scale to meet grid-scale storage needs.

Limitation of the study

In this section, we review the main limitations of our analysis. The scope of this work is to outline the necessary well properties needed to implement the REFRAES energy storage concept. The work provides a guide for well and surface machinery characteristics needed to provide round-trip energy storage efficiencies for diurnal and seasonal cycles. It does not provide grid-scale modeling, which could easily be a follow up study using the REFRAES idea. This study is limited to a single isolated hydraulically fractured well but with varying geological parameters informed by published data and state-of-the-artwell modeling software. The case studies for diurnal and seasonal storage scenarios are only given for symmetric cycles but could be extended to any cycle sequence in future studies. For simplicity of the model, we set the BHP to a constant during production cycles and used the average flow rate to calculate energy production. The average flow rate is within 10%–20% of the modeled flow rate for the majority (~80%) of the time. Leak-off from the reservoir was simulated using a constant pressure boundary by allowing gas to leak from the SRV to a large volume of unstimulated matrix outside of the SRV. No change in pressure (no leak-off) was observed from the SRV. We therefore did not include leak off in our sensitivity study.

STAR★METHODS

Detailed methods are provided in the online version of this paper and include the following:

- KEY RESOURCES TABLE
- RESOURCE AVAILABILITY
  - Lead contact
  - Materials availability
  - Data and code availability
- METHODS DETAILS
  - Reservoir dual porosity-model

ACKNOWLEDGMENTS

This work was authored by the National Renewable Energy Laboratory, operated by Alliance for Sustainable Energy, LLC, for the U.S. Department of Energy (DOE) under Contract No. DE-AC36-08GO28308. The views expressed in the article do not necessarily represent the views of the DOE or the U.S. Government. The U.S. Government retains and the publisher, by accepting the article for publication, acknowledges that the U.S. Government retains a nonexclusive, paid-up, irrevocable, worldwide license to publish or reproduce the published form of this work, or allow others to do so, for U.S. Government purposes. Funding provided by U.S. Department of Energy Office of Energy Efficiency and Renewable Energy Geothermal Technologies Office.

AUTHOR CONTRIBUTIONS

Conception, D.L.Y. and C.A.; Writing, D.L.Y., C.A., and H.J.; Reservoir Modeling, H.J. and C.A.; Borehole, surface model, C.A.; technoeconomic model, C.A. and D.L.Y., Review and Editing, C.A., H.J., and D.L.Y.

DECLARATION OF INTERESTS

The authors declare authorship of U.S. Patent US 11,161,694 B2 "COMPRESSED GAS ENERGY STORAGE", Augustine, Young, and Johnston, Nov. 2, 2021.

Received: June 2, 2021
Revised: October 14, 2021
Accepted: November 10, 2021
Published: December 17, 2021

REFERENCES

Albertus, P., Manser, J.S., and Litzelman, S. (2020). Long-duration electricity storage applications. Econ.Tech. *4*, 21–32. https://doi.org/10.1016/j.joule.2019.11.009.

Alternative Renewables Cost Assumptions in Annual Energy Outlook 2020 (2020). U.S Energy information administration. https://www.eia.gov/outlooks/aeo/pdf/AEO2020_IIF.pdf.

Atan, S., Ajayi, A., Honarpour, M., Turek, E., Dillenbeck, E., Mock, C., Ahmadi, M., and Pereira, C. (2018). The Viability of Gas Injection EOR in Eagle Ford Shale Reservoirs (Society of Petroleum Engineers), pp. 1–32, SPE-191673-MS.

Augustine, C., Johnston, H., Young, D.L., Amini, K., Uzun, I., and Hossein, K. (2021a). Evaluation of energy storage potential of unconventional shale reservoirs using numerical simulation of cyclic gas injection. J. Energy Resour. Technology *143*. https://doi.org/10.1115/1.4049736.

Augustine, C., Young, D.L., and Johnston, H. (2021b). Compressed gas energy storage. patent 11,161,694.

Birol, D.F. (2021). Net Zero by 2050, A Roadmap for the Global Energy Sector (International Energy Agency). www.iea.org.

Blakers, A., Stock, M., Lu, B., Cheng, C., and Stocks, R. (2019). Pathway to 100% renewable electricity. IEEE J. Photovoltaics *9*, 1828–1833. https://doi.org/10.1109/JPHOTOV.2019.2938882.

BNEF (2019). 2019 long-term energy storage outlook. https://www.bnef.com/core/insights/21113.

Center for Sustainable Systems (2020). U.S. Grid Energy Storage Factsheet (University of Michigan).

Computer Modeling Group (2017). CMG-GEM 2017.11 and CMG-WINPROP.

DOE (2021). U.S. Average Annual Wind Speed at 80 Meters. https://windexchange.energy.gov/maps-data/319.

Dong, Z., Holditch, S.A., McVay, D.A., Ayers, W.B., Lee, W.J., and Morales, E. (2014). Probabilistic assessment of world recoverable shale gas resources. In Paper presented at the SPE/EAGE European Unconventional Resources Conference and Exhibition, Vienna, Austria.

Energy Storage Association (2020). Mechanical energy storage - CAES. https://energystorage.org/why-energy-storage/technologies/mechanical-energy-storage/.

Fu, R., Remo, T., and Margolis, R. (2018). 2018 U.S. Utility-Scale Photovoltaics-Plus-Energy Storage System Costs Benchmark (National Renewable Energy Laboratory), NREL/TP-6A20-71714.

Gabrielli, P., Poluzzi, A., Kramer, G.J., Spiers, C., Mazzotti, M., and Gazzani, M. (2020). Seasonal energy storage for zero-emissions multi-energy systems via underground hydrogen storage. Renew. SustainableEnergy Rev. *121*, 109629. https://doi.org/10.1016/j.rser.2019.109629.

Gülen, S.C., Adams, S.S., Haley, R.M., and Carlton, C. (2017). Compressed gas energy storage. Energy Storage *123*, 22.

Gupta, U., and Turaga, U. (2021). Enter monster well-pads. https://adi-analytics.com/2019/11/12/enter-mega-pads-in-shale-drilling/.

Haegel, N.M., Atwater, H., Barnes, T., Breyer, C., Burrell, A., Chiang, Y.M., De Wolf, S., Dimmler, B., Feldman, D., Glunz, S., and Goldschmidt, J.C. (2019). Terawatt-scale photovoltaics: transform global energy. Science *364*, 836–838. https://doi.org/10.1126/science.aaw1845.

Hagoort, J. (2005). Prediction of wellbore temperatures in gas production wells. J. Pet. Sci. Eng. *49*, 22–36. https://doi.org/10.1016/j.petrol.2005.07.003.

Hughes, D.J. (2014). Drilling Deeper: A Reality Check on U.S. Government Forecasts for a Lasting Tight Oil & Shale Gas Boom (Post Carbon Institute).

Hydro Review Content Directors (2021). Pumped Storage Hydro, Utility-Scale Batteries Return about 80% of the Electricity They Store (U.S. Energy Information Adminstration). https://www.hydroreview.com/hydro-industry-news/pumped-storage-hydro-utility-scale-batteries-return-about-80-of-the-electricity-they-store/.

Kazemi, H., Eker, I., Torcuk, M.A., and Kurtoglu, B. (2015). Performance Analysis of Unconventional Shale Reservoirs, Fundamentals of Gas Shale Reservoirs (John Wiley & Sons, Ltd).

Kim, C. (2021). Oil, gas and mining left marks across Colorado. the federal infrastructure bill could help clean up some of it. https://www.cpr.org/2021/09/14/oil-gas-mining-cleanup-federal-infrastructure-bill/.

Kushnir, R., Ullmann, A., and Dayan, A. (2008). Steady periodic gas flow around a well of a CAES plant. Transp Porous Med. *73*, 1–20. https://doi.org/10.1007/s11242-007-9156-x.

Lake, L.W., Martin, J., Ramsey, J.D., and Titman, S. (2013). A primer on the economics of shale gas production just how cheap is shale gas? J. Appl. Corporate Finance *25*, 87–96.

Lemmon, E.W., Bell, I.H., Huber, M.L., and McLinden, M.O. (2018). NIST Standard Reference Database 23: Reference Fluid Thermodynamic and Transport Properties-REFPROP (National Institute of Standards and Technology).

Lund, L. (2014). Decline Curve Analysis of Shale Oil Production the Case of Eagle Ford (Master (Uppsala Universitet)).

Luo, X., Wang, J., Dooner, M., and Clarke, J. (2015). Overview of current development in electrical energy storagetechnologies and the application potential in power system operation. Appl. Energy *137*, 511–536. https://doi.org/10.1016/j.apenergy.2014.09.081.

Mouli-Castillo, J., Wilkinson, M., Mignard, D., McDermott, C., Haszeldine, R.S., and Shipton, Z.K. (2019). Inter-seasonal compressed-air energy storage using saline aquifers. Nat. Energy *4*, 131–139. https://doi.org/10.1038/s41560-018-0311-0.

Okouma, V., Guillot, M.S., San, V., Ilk, D., and Blasingame, T.A. (2011). Estimated ultimate recovery (EUR) as a function of production practices in the Haynesville shale. In aper presented at the SPE Annual Technical Conference and Exhibition (Denver, Colorado, USA).

Oldenburg, C.M., and Pan, L. (2013). Porous media compressed-air energy storage (PM-CAES): theory and simulation of the coupled wellbore–reservoir system. Transp Porous Med. *97*, 201–221. https://doi.org/10.1007/s11242-012-0118-6.

Radmax Technologies (2021). https://radmaxtech.com/.

Raziperchikolaee, S., and Mishra, S. (2019). Numerical simulation of CO2 huff and puff feasibility for light oil reservoirs in the appalachian basin: sensitivity study and history match of a CO2 pilot test. Energy Fuels *33*, 10795–10811. https://doi.org/10.1021/acs.energyfuels.9b02710.

Rezaee, R. (2015). Fundamentals of Gas Shale Reservoirs (Wiley).

Roberts, B.J. (2021). Global Horizontal Solar Irradiance, https://www.nrel.gov/gis/assets/images/solar-annual-ghi-2018-usa-scale-01.jpg.

Schmidt, O., Melchior, S., Hawkes, A., and Staffell, I. (2019). Projecting the future levelized cost of electricity storage technologies. Joule *3*. https://doi.org/10.1016/j.joule.2018.12.008.

Schulte, R.H., Nicholas Critelli, J., Holst, K., and Huff, G. (2012). Lessons from Iowa: Development of a 270 Megawatt Compressed Air Energy Storage Project in Midwest Independent System Operator, A Study for the DOE Energy Storage Systems Program (Sandia National Laboratory), January, SAND2012-0388.

Siddhamshetty, P., Wu, K., and Kwon, J.S.-I. (2019). Modeling and control of proppant distribution of multistage hydraulic fracturing in horizontal shale wells. Ind. Eng. Chem. Res. *58*, 10. https://doi.org/10.1021/acs.iecr.8b05654.

Succar, S., and Williams, R.H. (2008). Compressed air energy storage: theory, resources, and applications for wind power. Princeton Environ. Inst. Rep. *8*, 81.

Turrentine, J. (2021). Millions of leaky and abandoned oil and gas wells are threatening lives and the climate. https://www.nrdc.org/stories/millions-leaky-and-abandoned-oil-and-gas-wells-are-threatening-lives-and-climate.

US Energy Information Administration (2011). Review of emerging resources: U.S. shale gas and shale oil plays. https://www.eia.gov/analysis/studies/usshalegas/pdf/usshaleplays.pdf.

US Energy Information Administration (2019). The Distribution of U.S. Oil and Natural Gas Wells by Production Rate, (U.S. Department of Energy). https://www.eia.gov/petroleum/wells/pdf/full_report.pdf.

USGS (2021). Hydraulically Fractured Wells, https://www.usgs.gov/media/images/map-hydraulically-fractured-wells.

Uzun, I., Kurtoglu, B., and Kazemi, H. (2016). Multiphase Rate-Transient Analysis in Unconventional Reservoirs: Theory and Application, *19* (SPE Reservoir Evaluation & Engineering). SPE-171657-PA. https://doi.org/10.2118/171657-PA.

Uzun, I., Eker, E., Cho, Y., Kazemi, H., and Rutledge, J.M. (2017). Assessment of Rate Transient Analysis Techniques for Multiphase Flow in Unconventional Reservoirs: Application to Eagle Ford Formation (SPE Western Regional Meeting).

Vallourec (2014). Vallourectube-alloy vacuum insulated tubing. sales.vta-usa@vallourec.com.

Van Vuuren, D.P., Stehfest, E., Gernaat, D.E., Van Den Berg, M., Bijl, D.L., De Boer, H.S., Daioglou, V., Doelman, J.C., Edelenbosch, O.Y., Harmsen, M., and Hof, A.F. (2018). Alternative pathways to the 1.5°Ctarget reduce the need for negative emission technologies. Nat. Clim. Change *8*, 391–397. https://doi.org/10.1038/s41558-018-0119-8.

Wachtmeister, H., Lund, L., Aleklett, K., and Höök, M. (2017). Production decline curves of tight oil wells in eagle ford shale. Nat. Resour. Res. *26*, 365–377.

Warren, J.E., and Root, P.J. (1963). The behavior of naturally fractured reservoirs. SPE J. *3*, 245–255. https://doi.org/10.2118/426-PA.

Zhang, H.L., Baeyens, J., Degreve, J., and Caceres, G. (2013). Concentrated solar power plants: review and design methodology. Renew. Sustain. Energy Rev. *22*, 466–481.

STAR★METHODS

KEY RESOURCES TABLE

REAGENT or RESOURCE	SOURCE	IDENTIFIER
Deposited data		
Subsurface model output results	GDR	https://gdr.openei.org/submissions/1341, https://dx.doi.org/10.15121/1828157
Software and algorithms		
Equation-of-State (EoS) reservoir simulator for compositional, chemical, and unconventional reservoir modeling	CMG-GEM	https://www.cmgl.ca/gem
Borehole model	GDR	https://gdr.openei.org/submissions/1341, https://dx.doi.org/10.15121/1828157
Surface model	GDR	https://gdr.openei.org/submissions/1341, https://dx.doi.org/10.15121/1828157
Levelized-cost-of-storage calculations	GDR	https://gdr.openei.org/submissions/1341, https://dx.doi.org/10.15121/1828157

RESOURCE AVAILABILITY

Lead contact

Further information and requests for resources and reagents should be directed to and will be fulfilled by the lead contact, David Young (David.young@nrel.gov).

Materials availability

This study did not generate new unique reagents.

Data and code availability

Input files including all input data to subsurface, borehole and surface machinery models have been deposited at GDR and are publicly available as of the date of publication. Accession numbers are listed in the key resources table.

All original code has been deposited at GDR and is publicly available as of the date of publication. DOIs are listed in the key resources table.

Any additional information required to reanalyze the data reported in this paper is available from the lead contact upon request.

METHODS DETAILS

The full REFRAES model consists of three parts: 1) well bore; 2) reservoir; and 3) surface machinery. The LCOS model is described in detail in the text. The well bore and surface machinery models are thoroughly described in the main text, but the reservoir model was first described in detail in Augustine et al. (2021a). We therefore will provide details on the reservoir model here. For this study, we assumed that the shale gas reservoir was a dry-gas formation. We assumed that the dry-gas reservoir has been producing for at least a year and is partially depleted. The assumed reservoir pressure during energy storage operations will be significantly lower than the original reservoir pressure, and the well is depleted enough that we can assume the pressure field around the well and fractures is nearly uniform. First, we developed a conceptual model of a hydraulically fractured reservoir using data from literature when possible to study reservoir behavior during cyclic operation. We validated the model by minimizing numerical effects and comparing the results to analytical solutions. We performed sensitivity analyses to determine the major factors controlling reservoir performance. Finally, we updated the model to simulate the energy-storage cycle for the Marcellus shale gas formation.

Reservoir dual porosity-model

Numerical reservoir models of a multistage, hydraulically fractured, horizontal gas well were built using the commercial software CMG-GEM, which is an Equation-of-State (EoS) reservoir simulator for compositional, chemical, and unconventional reservoir modeling (Computer Modeling Group, 2017). This model can accommodate dry-gas, wet-gas, and liquid systems as a multicomponent, dual-porosity reservoir.

The modeled reservoir consists of a horizontal well with multistage fractures. Our conceptual model uses parameter values typical for unconventional shales compiled from a sampling of unconventional shale reservoirs, wells, hydraulic fractures, and SRVs and from the authors' experience working in shale gas formations. All input data files are deposited at GDR (and are listed in table form in Augustine et al.(2020)). We assumed that the reservoir fluid is a dry gas with the composition given in the input data files.

The Peng-Robinson equation of state was used in CMG WinProp (code deposited in the GDR), an EOS tool to model phase behavior and fluid properties, to model the fluid properties of the gas phase. WinProp provided default properties for the seven components in the gas phase. Properties provided for each component include critical pressure, critical temperature, acentric factor, molecular weight, critical volume, specific gravity, average normal boiling point, heating value, binary interaction coefficients, parachor values, and enthalpy coefficients. The solubility of each gas phase component in the aqueous phase was modeled using Henry's Law.